INT. J. NUM. METH. HEAT FLUID FLOW, VOL. 4, 497–511 (1994)

# NUMERICAL REALIZATION OF BLOW-UP SPIRAL WAVE SOLUTIONS OF A NONLINEAR HEAT-TRANSFER EQUATION

STEFKA N. DIMOVA† AND DANIELA P. VASILEVA‡

†*Faculty of Mathematics and Informatics, University of Sofia, Sofia 1126, Bulgaria*
‡*Institute of Mathematics, Bulgarian Academy of Sciences, Sofia 1113, Bulgaria*

## ABSTRACT

The problem of finding the possible classes of solution of different nonlinear equations seems to be of a great importance for many applications. In the context of the theory of self-organization it is interpreted as finding all possible structures which arise and preserve themselves in the corresponding unbounded nonlinear medium. First, results on the numerical realization of a class of blow-up invariant solutions of a nonlinear heat-transfer equation with a source are presented in this article. The solutions considered describe a spiral propagation of the inhomogeneities in the nonlinear heat-transfer medium. We have found initial perturbations which are good approximations to the corresponding eigen functions of combustion of the nonlinear medium. The local maxima of these initial distributions evolve consistent with the self-similar law up to times very close to the blow-up time.

KEY WORDS Combustion Nonlinear heat-transfer equation Blow-up Spiral wave solution Finite element method

## INTRODUCTION

The existence of spiral waves is a common property of many open, nonlinear systems. Spiral waves are observed experimentally in certain two-dimensional chemical and biological systems[1,2]. During the last 15 years many specialists have studied the existence and the behaviour of spiral-wave solutions of the mathematical models of such systems. For example, spiral wave solutions are obtained and analyzed for reaction-diffusion systems[3,4], $\lambda$–$\omega$ systems[5], the Kuramoto–Tsuzuki equation[6,7] and the Ginsburg–Landau equation[8]. In the Ph.D. Thesis of S. R. Svirshchevskii (1985) blow-up spiral wave solutions of the nonlinear heat-transfer equation with a source:

$$u_t=\frac{1}{r}(ru^{\sigma}u_r)_r+\frac{1}{r^2}(u^{\sigma}u_{\varphi})_{\varphi}+u^{\beta}, \qquad t>0, \qquad 0<r<\infty, \qquad 0<\varphi<2\pi \tag{1}$$

were found by the method of invariant-group analysis, but their numerical realization was until now an unsolvable problem. Equation (1) models the combustion of a two-dimensional nonlinear medium with parameters $\sigma>0$, $\beta>1$ in polar coordinates. It is one of the simplest models of open nonlinear systems and hence, very important to investigate.

0961–5539/94/060497–15$2.00


*Received December 1992*
*Revised October 1993*

The above mentioned invariant solution is[9-11]:

$$u_o(t,r,\varphi)=(1-t/T_o)^{-1/(\beta-1)}\theta(\xi,\phi), \tag{2}$$

$$\xi=\frac{r}{(1-t/T_o)^m}, \qquad m=\frac{\beta-\sigma-1}{2(\beta-1)}, \qquad \phi=\varphi+\frac{C_o}{\beta-1}ln(1-t/T_o)$$

Here, $T_o$ is the blow-up time, $C_o$ is a parameter of the family of solutions, the function $\theta(\xi,\phi)\geqslant 0$ satisfies the following nonlinear elliptic equation:

$$\frac{1}{\xi}(\xi\theta^\sigma\theta_\xi)_\xi+\frac{1}{\xi^2}(\theta^\sigma\theta_\phi)_\phi-\frac{\beta-\sigma-1}{2(\beta-1)T_o}\xi\theta_\xi+\frac{C_o}{(\beta-1)T_o}\theta_\phi-\frac{1}{(\beta-1)T_o}\theta+\theta^\beta=0, \quad 0<\xi<\infty, \quad 0<\phi<2\pi \tag{3}$$

The functions $\theta(\xi,\phi)$ defining the space-time structure of the invariant solutions (2) are said to be *eigen functions of combustion*[12] of the nonlinear medium, described by equation (1). Without loss of generality we set $T_o=(\beta-1)^{-1}$ and then equation (3) will have $\theta_H\equiv 1$ as homogeneous solution.

The case $C_o=0$ is analyzed in[13-15]. Complex symmetries solutions (different from radially symmetrical) of equation (3) for $C_o=0$ are found there and numerical methods for computation of such solutions are proposed.

This paper is devoted to the numerical investigation of the combustion of the medium which is consistent with the non-radially symmetrical solutions (2) when $C_o\neq 0$. As mentioned in [9,10], if at the initial time the temperature profile has inhomogeneities (for example, local maxima) then their trajectories will be logarithmic spirals—denoting by $(r(t), \varphi(t))$ the coordinates of such an inhomogeneity at time $t$ we get:

$$r(t)e^{s\varphi(t)}=r(0)e^{s\varphi(0)}, \qquad s=\frac{\beta-\sigma-1}{2C} \tag{4}$$

It is clear that the propagation direction for fixed $C_o$ depends on the relation between $\sigma$ and $\beta$: for $\beta<\sigma+1$ (the so-called HS evolution[9,12]) the movement is directed from the centre along the spiral, for $\beta>\sigma+1$ it is directed towards the centre (LS evolution). At $\beta=\sigma+1$ (S evolution) the spirals degenerate into circles.

The numerical experiments show, that it is not possible to realize a spiral propagation of the inhomogeneities in the nonlinear heat-transfer medium taking arbitrary initial data. That is why, as it is noted in[11], a very important, but difficult problem is the construction of the eigen functions $\theta(\xi,\phi)$. Here we propose and calculate some approximations to $\theta(\xi,\phi)$ and investigate their evolution in time.

Subsequently we linearize equation (3) with respect to the homogeneous solution $\theta_H\equiv 1$. We find particular solutions of the form $Y_k(\xi,\phi)=R_k(\xi)e^{ik\phi}$, where $k$ is an integer, of the linear equation obtained. It occurs that $R_k(\xi)$ are the Bessel functions of a complex variable $(\beta=\sigma+1)$ or the confluent hypergeometric function of a complex parameter $(\beta\neq\sigma+1)$. We investigate the structure of the linearized approximations depending on the parameters $\sigma$, $\beta$, $C_o$ and $k$.

We analyze, numerically, the evolution in time of the linearized approximations in the case when $\beta<\sigma+1$. The numerical experiments show that if these approximations are close to $\theta_H$ they are 'almost' the sought-after eigen functions. Then the evolution of their maxima is consistent with the law (4) up to times very close to the blow-up time.

We describe the numerical method used for solving the problem (1) with the appropriate boundary and initial conditions. It is the semidiscrete finite element method with interpolation of the nonlinear coefficients and lumped mass matrix. To solve the resulting system of ordinary differential equations in time, we use an explicit method with control of the accuracy and the relative stability and an automatic choice of the time step. Two special modifications of the method are made in order to satisfy the periodic boundary conditions and to ensure that $u(t,0,\varphi)$

does not depend on $\varphi$. The verification of the proposed method is achieved by solving two model problems with known solutions—a non-singular in time solution and a singular one.

## LINEARIZED EQUATION AND ITS PARTICULAR SOLUTIONS

In order to describe the behaviour of the eigen functions in the region where they are non-monotonic, we use the proposed linearization method in[12–14] with respect to the homogeneous solution $\theta_H \equiv 1$. This approach is based on the hypothesis that in some region the oscillations of the eigen functions $\theta(\xi,\phi)$ near $\theta_H$ are small:

$$\theta(\xi,\phi)=1+\alpha y(\xi,\phi), \qquad |\alpha y| \ll 1$$

$\alpha$ is a parameter. Introducing this in (3) and keeping only the linear terms in $\alpha y$ we obtain:

$$\frac{1}{\xi}(\xi y_\xi)_\xi+\frac{1}{\xi^2}y_{\phi\phi}-\frac{\beta-\sigma-1}{2}\xi y_\xi+C_o y_\phi+(\beta-1)y=0 \tag{5}$$

We seek particular solutions of the kind:

$$Y_k(\xi,\phi)=R_k(\xi)e^{ik\phi} \tag{6}$$

In order to have $Y_k(\xi,\phi)=Y_k(\xi,\phi+2\pi)$ the parameter $k$ should be integer. The radially-symmetric case corresponds to $k=0$ and it is investigated in[9,12,16]. In what follows we assume $k\neq 0$. The function $R_k(\xi)$ satisfies the equation:

$$R_k''+\left(\frac{1}{\xi}-\frac{\beta-\sigma-1}{2}\xi\right)R_k'+\left(-\frac{k^2}{\xi^2}+C_o ki+\beta-1\right)R_k=0 \tag{7}$$

We seek solutions of (7) only for $k>0$ because, if $R_k(\xi;C_o)$ is a solution for fixed $k$ and $C_o$, it is also a solution for $-k$ and $-C_o$—i.e. we can choose:

$$R_k(\xi,C_o)=R_{-k}(\xi,-C_o), \qquad k<0 \tag{8}$$

Looking for bounded at $\xi=0$ solutions, we find:

For $\beta=\sigma+1$

$$R_k(\xi)=J_k(z), \qquad z=(\sigma+C_o ki)^{1/2}\xi \tag{9}$$

where $J_k(z)$ is the Bessel function of the first kind of order $k$.

For $\beta\neq\sigma+1$

$$R_k(\xi)=\xi^k\,{}_1F_1(a,b,z) \tag{10}$$

$$a=-\frac{\beta-1+C_o ki}{\beta-\sigma-1}+\frac{k}{2}, \qquad b=1+k, \qquad z=\frac{\beta-\sigma-1}{4}\xi^2$$

where ${}_1F_1(a,b,z)$ is the confluent hypergeometric function.

The corresponding solutions $Y_k(\xi,\phi)$ are complex, but their real and imaginary parts (and any linear combination of theirs) are solutions of (5) too. Note that $Y_k(0,\phi)=\text{const}$ is a natural condition when polar coordinates are used (in our case $Y_k(0,\phi)=0$, $k\neq 0$). We investigate only the real part of (6) because from the representation:

$$Y_k(\xi,\phi)=|R_k(\xi)|e^{i\omega(\xi)}e^{ik\phi}=|R_k(\xi)|[\cos(\omega(\xi)+k\phi)+i\sin(\omega(\xi)+k\phi)], \qquad \omega(\xi)=\arg(R_k(\xi)) \tag{11}$$

it follows that:

$$\alpha_1 \mathbb{R}e(Y_k(\xi,\phi))+\alpha_2 \mathbb{I}m(Y_k(\xi,\phi))=(\alpha_1^2+\alpha_2^2)^{1/2}\mathbb{R}e(Y_k(\xi,\psi))$$

where $\psi=\phi+\frac{\gamma}{R}$, $\quad cos\gamma=\frac{\alpha_1}{(\alpha_1^2+\alpha_2^2)^{1/2}}$, $\quad sin\gamma=\frac{-\alpha_2}{(\alpha_1^2+\alpha_2^2)^{1/2}}$

Let $y_k(\xi,\phi)=\mathbb{R}e(Y_k(\xi,\phi))$ and let us denote by $y_k(\xi,\phi;C_o)$ the solution $y_k(\xi,\phi)$ of (5) for fixed $C_o$. Using (11) it is easy to obtain:

$$y_k\left(\xi,\phi+\frac{2}{k}\pi\right)=y_k(\xi,\phi), \qquad y_k\left(\xi,\phi+\frac{\pi}{k}\right)=-y_k(\xi,\phi) \tag{12}$$

Further from the relationships:

$$J_k(z)=\overline{J_k(\bar{z})}, \qquad {}_1F_1(a,b,z)=\overline{{}_1F_1(\bar{a},b,z)}$$

and (8) we get:

$$y_k(\xi,\phi;C_o)=y_k(\xi,-\phi;-C_o)=y_{-k}(\xi,\phi;C_o)=y_k(\xi,-\phi;-C_o)$$

That is why we only examine the case $k>0$, $C_o>0$.

Asymptotic expansions of $J_k(z)$ and ${}_1F_1(a,b,z)$ yield the formulas[17,18]:

$$J_k(z)=\left(\frac{2}{\pi z}\right)^{1/2}\left[cos\left(z-\frac{k}{2}\pi-\frac{\pi}{4}\right)+e^{|\Im m(z)|}O(|z|^{-1})\right] \tag{13}$$

$$|z|\to\infty, \qquad |arg(z)|<\pi$$

$${}_1F_1(a,b,z)=\frac{\Gamma(b)e^{i\pi a}z^{-a}}{\Gamma(b-a)}\left[\sum_{m=0}^{R-1}\frac{(a)_m(1+a-b)_m}{m!}(-z)^{-m}+O(|z|^{-R})\right]$$

$$+\frac{\Gamma(b)e^{z}z^{a-b}}{\Gamma(a)}\left[\sum_{n=0}^{s-1}\frac{(b-a)_n(1-a)_n}{n!}z^{-n}+O(|z|^{-S})\right] \tag{14}$$

$$|z|\to\infty, \qquad -\frac{\pi}{2}<arg(z)<\frac{3}{2}\pi, \qquad (a)_m=a(a+1)\ldots(a+m-1), \qquad (a)_0=1, \text{ or}$$

$${}_1F_1(a,b,z)\sim\frac{\Gamma(b)}{\Gamma(a)}e^{z}z^{a-b}, \qquad \mathbb{R}e(z)\to\infty \tag{15}$$

$${}_1F_1(a,b,z)\sim\frac{\Gamma(b)}{\Gamma(b-a)}(-z)^{-a}, \qquad \mathbb{R}e(z)\to\infty \tag{16}$$

Hence if $\beta<\sigma+1$ using (16) we get $|R_k(\xi)|_{\xi\to\infty}\to 0$. When $\beta=\sigma+1$ (and $C_0k\neq 0$) or $\beta>\sigma+1$ it follows from (13) or (15) respectively that $|R_k(\xi)|_{\xi\to\infty}\to\infty$. If $\beta=\sigma+1$ and $C_0k=0$ then $|R_k(\xi)|_{\xi\to\infty}\to 0$.

*In Figure 1* the contours of some of the functions $y_k(\xi,\phi)$ for different parameters $\sigma$, $\beta$, $C_0$ and $k$ are shown (in Cartesian coordinates). *Figure 1a* to *1f* illustrate the case $\beta<\sigma+1$, *Figure 1g*—$\beta=\sigma+1$, *Figure 1h*—$\beta>\sigma+1$.

*Figure 1a* to *1c* show the evolution of the shape of $y_k(\xi,\phi)$ depending on the parameter $C_0$ ($C_0=0;0.1;1$); the other parameters are $\sigma=2$, $\beta=2.4<\sigma+1$, $k=2$ (two-armed spirals). *Figure 1d* shows the one-armed spiral (k = 1) for the same $\sigma$, $\beta$ and $C_0=1$ and *Figure 13*—the three-armed spiral for $C_0=0.5$. The one-armed spiral in *Figure 1f* is for $\sigma=2$, $\beta=2.8$, $C_0=1$. *Figure 1g* and *Figure 1h* show the one-armed spirals for $\sigma=2$, $C_0=1$, $\beta=3=\sigma+1$ and $\beta=3.4>\sigma+1$, respectively. These and the other experiments we have done show how the structure of the linearized approximations depend on the parameters $\sigma$, $\beta$, $C_0$ and $k$. For a fixed $k$ and $\beta<\sigma+1$ the density and the core of the spirals increase with $C_0$ or when $\beta\to\sigma+1-0$. The core of a spiral is the circle $V_{\xi_0}(0)$ of radius $\xi_0$ around the origin, out of which:

$$|R_k(\xi)|<\delta\cdot\max_{\xi}|R_k(\xi)|, \qquad \xi>\xi_0, \tag{17}$$

for some small $\delta$. For $\beta \geqslant \sigma+1$ the density of the spirals increases with $C_0$ or when $\beta \to \sigma+1+0$ and the cores of the spirals are infinite. For fixed $\sigma$, $\beta$, $C_0$ the density and the maxima of the spirals increase with $k$. The spirals are not logarithmic, but for $\beta<\sigma+1$ ($\beta>\sigma+1$) and large $\xi$ they are close to the logarithmic spirals with parameter $s$ ($-s$) defined in (4). For $\beta=\sigma+1$ and large $\xi$ they are the Archimedean ones.

To calculate $J_k(z)$ and ${}_1F_1(a,b,z)$ for complex values of $z$ and $a$ respectively, we worked out two algorithms. The first one is based on the expansions[17]:

$$J_k(z)=\frac{(z/2)^k}{\Gamma(k+1)}\sum_{n=0}^{\infty}\frac{(-z^2/4)^n}{(k+1)_n n!}$$

$${}_1F_1(a,b,z)=\sum_{n=0}^{\infty}\frac{(a)_n z^n}{(b)_n n!} \text{ for } \beta>\sigma+1,$$

and on the formula[17]:

$${}_1F_1(a,b,z)=e^z\,{}_1F_1(b-a,b,-z) \text{ for } \beta<\sigma+1.$$

We use the expansion for ${}_1F_1(b-a,b,-z)$ because in this case the expansion for ${}_1F_1(a,b,z)$ has very large alternating terms.

The second algorithm is based on some rational approximations. For $\beta=\sigma+1$ we use the approximations[19]:

$$I_k(z)=\frac{e^z\varphi_k^{(n)}(z)}{\Omega^{(n)}(z)}+R_k^{(n)}(z), \qquad R_k^{(n)}(z)_{n\to\infty}\to 0, \qquad -\pi<arg(z)\leqslant\pi,$$

$$\varphi_{n+2}^{(n)}=0, \qquad \varphi_{n+1}^{(n)}=1, \qquad \varphi_m^{(n)}(z)=2(m+1)\varphi_{m+1}^{(n)}(z)/z+\varphi_{m+2}^{(n)}(z), \qquad m=n,n-1,\ldots,0.$$

$$\Omega^{(n)}(z)=\varphi_0^{(n)}(z)+2\sum_{m=1}^{n+1}\varphi_m^{(n)}(z)$$

and the relationship[17]:

$$J_k(z)=e^{ik\pi/2}I_k(ze^{-i\pi/2}), \qquad -\pi/2<arg(z)\leqslant\pi$$

For $\beta\neq\sigma+1$ we use[18]:

$${}_1F_1(a,b,z)=A_n(z)/B_n(z)+R_n(z)$$

$$B_n(z)=\sum_{m=0}^{n}A_{n,m}z^{-m}, \qquad A_{n,m}=\frac{(-n)_m(n+\lambda)_m(b-\varepsilon)_m}{(\beta+1)_m(a+1-\varepsilon)_m}, \qquad \lambda>\beta>-1, \qquad \varepsilon=0 \text{ or } 1$$

$$A_n(z)=z^{-\varepsilon}\sum_{m=0}^{n-\varepsilon}\frac{(a)_m}{(b)_m m!}\sum_{r=0}^{n-m-\varepsilon}A_{n,r+m+\varepsilon}z^{-r}$$

We also checked our results for large $\xi$ with the asymptotic expansions (13), (14).

## EVOLUTION OF THE LINEARIZED APPROXIMATIONS

The analysis of the structure and the behaviour of the linearized approximations shows that the assumption for small oscillations of the eigen functions near $\theta_H=1$ might be correct only in the case when $\beta<\sigma+1$. That is why we examine only the evolution in time of these linearized approximations.

Let us note that in the radially symmetrical case for $\beta\leqslant\sigma+1$ (as proved in[12]) a continuous set of eigen functions tending at infinity to the homogeneous solution $\theta_H$ exists. It seems that for $\beta<\sigma+1$ there exists a continuous set of non-symmetric solutions as well.

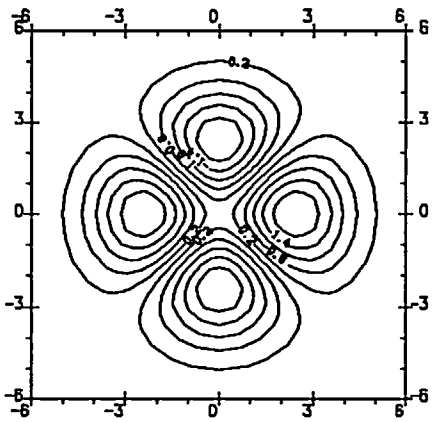

(a) $\sigma=2,\ \beta=2.4,\ k=2,\ C_0=0$

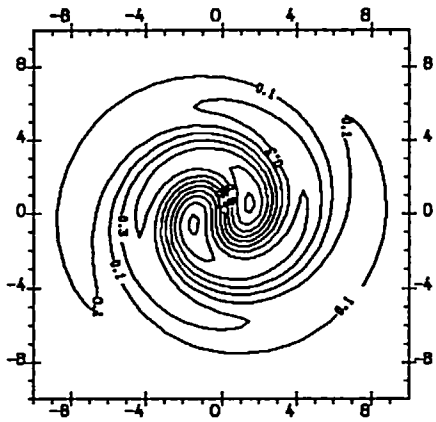

(d) $\sigma=2,\ \beta=2.4,\ k=1,\ C_0=1$

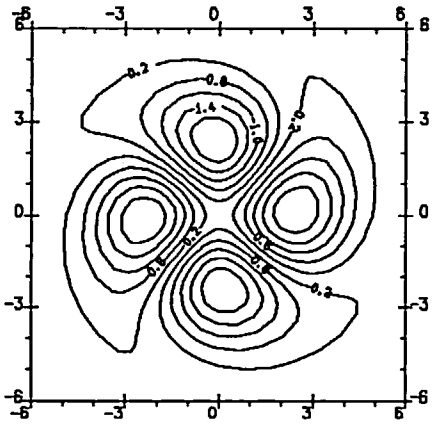

(b) $\sigma=2,\ \beta=2.4,\ k=2,\ C_0=0.1$

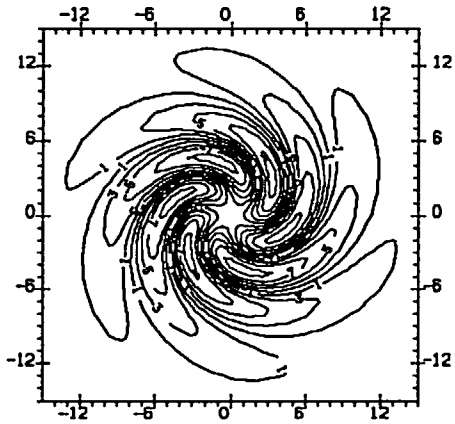

(e) $\sigma=2,\ \beta=2.4,\ k=3,\ C_0=0.5$

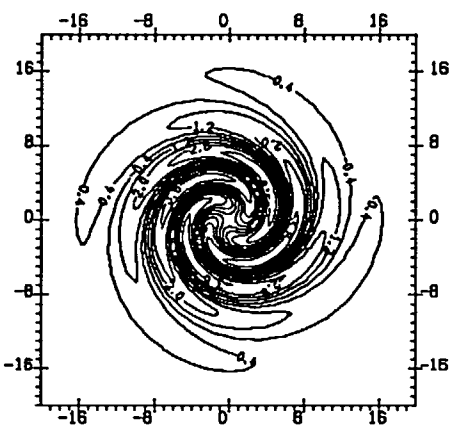

(c) $\sigma=2,\ \beta=2.4,\ k=2,\ C_0=1$

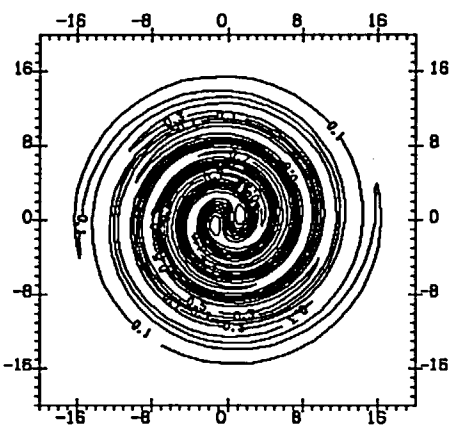

(f) $\sigma=2,\ \beta=2.8,\ k=1,\ C_0=1$

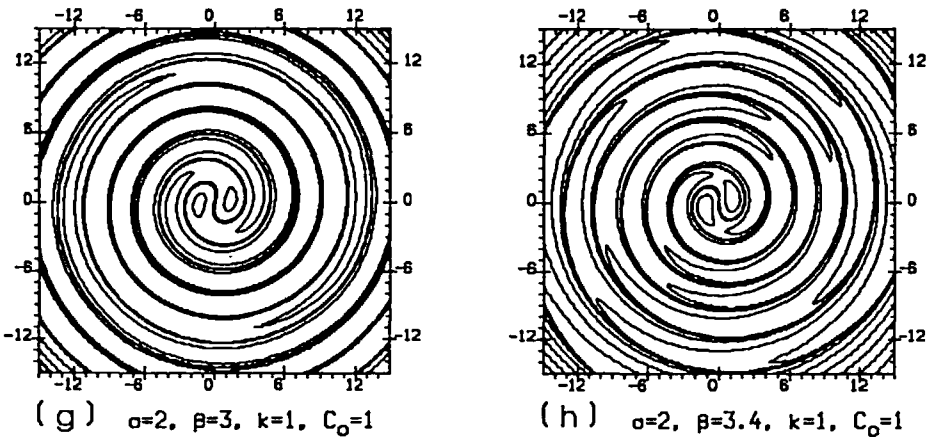


*Figure 1* Contours of some of the linearized approximations

Let:

$$\tilde{\theta}_k(r,\varphi)=\begin{cases}1+\alpha y_k(r,\varphi), & 0\leqslant r<r_0, \quad 0\leqslant\varphi\leqslant 2\pi,\\ \vartheta, & r\geqslant r_0, \quad 0\leqslant\varphi\leqslant 2\pi,\end{cases} \tag{18}$$

where $y_k(r,\varphi)=|R_k(r)|cos(arg(R_k(r)+k\varphi))$, $R_k$ is given by (9) or (10), $\alpha$, $\vartheta$ and $r_0$ are constants. In the examples below $r_0$ is chosen so that the circle $V_{r_0}(0)$ is the core of the spiral for $\delta=0.01$ (see (17)).

We solve, numerically, the initial boundary-value problem:

$$u_t=\frac{1}{r}(ru^\sigma u_r)_r+\frac{1}{r^2}(u^\sigma u_\varphi)_\varphi+u^\beta, \qquad 0<t<T_0, \qquad (r,\varphi)\in\Omega \tag{19}$$

$$\Omega=(0,R)\times\left(0,\frac{2}{k}\pi\right),$$

$$ru^\sigma u_r(t,0,\varphi)=0 \text{ for } t\in[0,T_0), \qquad \varphi\in\left[0,\frac{2}{k}\pi\right] \tag{20}$$

$$u^\sigma u_r(t,R,\varphi)=0 \text{ for } t\in[0,T_0), \qquad \varphi\in\left[0,\frac{2}{k}\pi\right] \tag{21}$$

$$u(t,r,0)=u\left(t,r,\frac{2}{k}\pi\right), \qquad \text{for } t\in[0,T_0), \qquad r\in[0,R] \tag{22}$$

$$u^\sigma(t,r,0)u_\varphi(t,r,0)=u^\sigma\left(t,r,\frac{2}{k}\pi\right)u_\varphi\left(t,r,\frac{2}{k}\pi\right) \tag{23}$$

$$\text{for } t\in[0,T_0), \qquad r\in[0,R]$$

$$u(0,r,\varphi)=u_0(r,\varphi)\geqslant 0, \qquad (r,\varphi)\in\bar{\Omega} \tag{24}$$

$$u_0(0,\varphi)=const, \qquad u_0(r,0)=u_0\left(r,\frac{2}{k}\pi\right), \qquad u_{0,\varphi}(r,0)=u_{0,\varphi}\left(r,\frac{2}{k}\pi\right) \tag{25}$$

We choose the length $R=R(t)\gg r_0$ so as to avoid the influence of the boundary condition (21) on the numerical solution. Note, $\tilde{\theta}$ defined by (18) satisfies (25) and, therefore, it can be chosen as initial data.

Let us introduce the self-similar representation $\Theta(t,\xi,\phi)$ of the solution $u(t,r,\varphi)$ corresponding to the initial data $u_0(r,\varphi)$:

$$\Theta(t,\xi,\phi)=u(t,r,\varphi)/\gamma(t)$$
$$\xi=r\gamma(t)^{(\beta-\sigma-1)/2}, \qquad \phi=\varphi-C\cdot^0 ln(\gamma(t))$$
$$\gamma(t)=\sup_{\Omega} u(t,r,\varphi)/\sup_{\Omega} u_0(r,\varphi)$$

If $u_0(\xi,\phi)$ is an eigen function it is obvious that

$$\Theta(t,\xi,\phi)=u_0(\xi,\phi), \qquad t\in[0,T_0) \tag{26}$$

Moreover, if (26) holds then $u_0(r,\varphi)$ will be an eigen function.

In the following examples, some of the linearized approximations $\tilde{\theta}_k(r,\varphi)$ are chosen as initial data. For sufficiently small values of the parameter $\alpha$ they are 'almost' eigen functions in the sense of (26) and the corresponding blow-up times $\tilde{T}_0$ are approximately equal to the exact blow-up time $T_0=(\beta-1)^{-1}$. By $\tilde{T}_0$ the time reached in calculations is denoted assuming that the stop-criterion is $\tau<10^{-16}$, $\tau$ being the time step. Of course (26) is not satisfied exactly due to the following three reasons:

- $\tilde{\theta}_k(r,\varphi)$ is an approximation to some of the eigen functions;
- the problem is solved numerically;
- the self-similar solution (2) is not stable in Lyapunov's sense and probably it is not structurally stable. The self-similar solution, corresponding to the eigen function $\theta(\xi,\phi)$ is called *structurally stable*[12] if there exists a class of initial perturbations $u_0(r,\varphi)\neq\theta(r,\varphi)$, so that for their self-similar representations $\Theta(t,\xi,\phi)$ it holds:

$$\|\Theta(t,\xi,\phi)-\theta(\xi,\phi)\|\to 0, \qquad t\to T_0$$

*Example 1*

The function $\tilde{\theta}_k(r,\varphi)$ with parameters $\sigma=2$, $\beta=2.4$, $k=1$, $C_0=1$, $\alpha=0.01$, $\vartheta=1$ is used as initial data. The evolution in time of this linearized approximation is shown in *Figure 2*. The calculated blow-up time $T_0=0.714304$ is very close to the exact self-similar blow-up time $T_0=1/(\beta-1)=0.714285$. In *Figure 3a* the positions at some times of the local maximum of $\tilde{\theta}_k(r,\varphi)$ are marked—for $0<t<0.7128=99.79\%\ \tilde{T}_0$ they are the nearest meshpoints to the drawn self-similar trajectory (4). On the asymptotic stage the maximum stops and the solution grows as a radially symmetrical solution. This asymptotic behaviour is observed in all of the following examples.

Let us define the error:

$$\Delta\theta(t,\xi,\phi)=|\Theta(t,\xi,\phi)-\tilde{\theta}_k(\xi,\phi)|$$

*Table 1* contains the maximum of the solution, the errors $\Delta\theta_i$, $i=1,\ldots,4$, and the ratio $t/\tilde{T}_0$ for different times $t$. By $\Delta\theta_i$, $i=1,2,3$, the errors at the point of the minimum of the solution, at the origin and on the boundary ($r=R(t)$) are denoted, $\Delta\theta_4$ is the maximal value of $\Delta\theta$ in the core of the spiral for $\delta=0.1$. Let us note that $\Delta\theta_4<0.01\left(\max_{\Omega}\tilde{\theta}-\theta_H\right)$ for $0<t<0.5345=74.83\%\ \tilde{T}_0$. This fact, the excellent re-establishment of the blow-up time and the self-similar law of motion of the maximum allow us to assume that the initial perturbation $\tilde{\theta}_k(r,\varphi)$ is an 'almost' eigen function.

*Example 2*

Here we analyze what happens if we increase the value of $\alpha$. For $\alpha=0.1$ the calculated blow-up time $\tilde{T}_0=0.7138$ is close to the exact blow-up time $T_0$, for $\alpha=1$ it differs essentially from $T_0-\tilde{T}_0=0.5878$. In *Figure 3b* and *3c* the trajectories of the maximum of the solution for $\alpha=0.1$

*Table 1* Comparison between the self-similar representation and the linearized approximation for *Example* 1

| $t$ | $u_{max}$ | $\Delta\theta_1$ | $\Delta\theta_2$ | $\Delta\theta_3$ | $\Delta\theta_4$ | $t/\tilde{T}_0$ |
|---|---|---|---|---|---|---|
| 0.000000 | 1.0094 | $0.0\cdot10^{0}$ | $0.0\cdot10^{0}$ | $0.0\cdot10^{0}$ | $0.0\cdot10^{0}$ | 0.0000% |
| 0.170535 | 1.2265 | $1.9\cdot10^{-5}$ | $2.5\cdot10^{-5}$ | $3.8\cdot10^{-6}$ | $2.9\cdot10^{-5}$ | 23.8743% |
| 0.398423 | 1.8079 | $3.6\cdot10^{-5}$ | $4.2\cdot10^{-5}$ | $3.1\cdot10^{-5}$ | $5.3\cdot10^{-5}$ | 55.778% |
| 0.534493 | 2.7040 | $4.8\cdot10^{-5}$ | $4.4\cdot10^{-5}$ | $8.9\cdot10^{-5}$ | $9.6\cdot10^{-5}$ | 74.8271% |
| 0.672251 | 7.6359 | $2.7\cdot10^{-4}$ | $6.0\cdot10^{-6}$ | $4.8\cdot10^{-4}$ | $1.0\cdot10^{-3}$ | 94.1127% |
| 0.712678 | 78.243 | $1.0\cdot10^{-2}$ | $8.2\cdot10^{-4}$ | $4.2\cdot10^{-3}$ | $1.1\cdot10^{-2}$ | 99.7724% |
| 0.714301 | 8761.5 | $4.7\cdot10^{-1}$ | $1.0\cdot10^{-1}$ | $3.9\cdot10^{-1}$ | $4.7\cdot10^{-1}$ | 99.9996% |

and $\alpha=1$, respectively, are shown. In spite of the fact, that for $\alpha=1$ the initial data differ essentially from the homogeneous solution, the maximum moves along the self-similar logarithmic spiral for $0<t<0.3987=67.83\%\ \tilde{T}_0$.

*Example 3*

This is an example of a finite initial perturbation ($\vartheta=0$) whose maximum moves in consistency with the self-similar law up to time $0.3949=67.15\%\ \tilde{T}_0$, $\tilde{T}_0=0.5881$. In this case $\alpha=1$, the other parameters are as in the previous examples. The law of motion of the maximum is the same as for $\vartheta=1$ (see *Figure 3c*). Almost the same are the values of both solutions in the point of the maximum and in the centre of the spiral on the same times. This independence of the core of the solution from the space-homogeneous part is also observed in the *Example 5*.

*Example 4*

*Figure 3d* shows the motion of the maxima of $\tilde{\theta}_k(r,\varphi)$ for $\sigma=2$, $\beta=2.8$, $k=1$, $C_0=1$, $\alpha=0.01$, $\vartheta=1$. The blow-up time obtained is $\tilde{T}_0=0.55546\approx T_0=0.5$. For $0<t<0.5536=99.65\%\ \tilde{T}_0$ the maxima are on the corresponding self-similar trajectories. The first and the second maximum disappear at times 0.555477 and 0.5549, respectively. If by $\Delta\theta_4$ the maximal value of $\Delta\theta$ in the core of the spiral for $\delta=0.1$ is denoted, then $\Delta\theta_4<0.01\left(\max_{\Omega}\tilde{\theta}_k-\theta_H\right)$ for $0<t<0.3576=64.37\%\ \tilde{T}_0$. Hence, we think $\tilde{\theta}_k(r,\varphi)$ is also close to an eigen function.

*Example 5*

Here $\alpha=1$, $\vartheta=0$ or 1, the other parameters are as *Example 4*. It is another example where the inital perturbation is far from an eigen function, but the motion of the maxima follows the self-similar law for $0<t<0.3481=90.53\%\ \tilde{T}_0$ (see *Figure 3e*). The first of the maxima disappears at time 0.3820, the second 'dies' in comparison with the third when $t\to\tilde{T}_0=0.3845$.

## NUMERICAL METHOD FOR SOLVING THE PARABOLIC PROBLEM

The weak form of the problem (19)–(24) is:

Find $u(t,r,\varphi)\in C(0,T_0)\times D$:

$$D=\{w:\ r^{1/2}w,\qquad r^{1/2}\frac{\partial w^{q+1}}{\partial r},\qquad r^{-1/2}\frac{\partial w^{q+1}}{\partial\varphi}\in L_2(\Omega)\}$$

which satisfies the boundary conditions (20)–(23) and:

$$(u_t,v)+A(t;u,v)=(f,v)\ \text{for}\ \forall v\in H,\qquad 0<t<T_0$$

$$u(0,.,.)=u_0$$

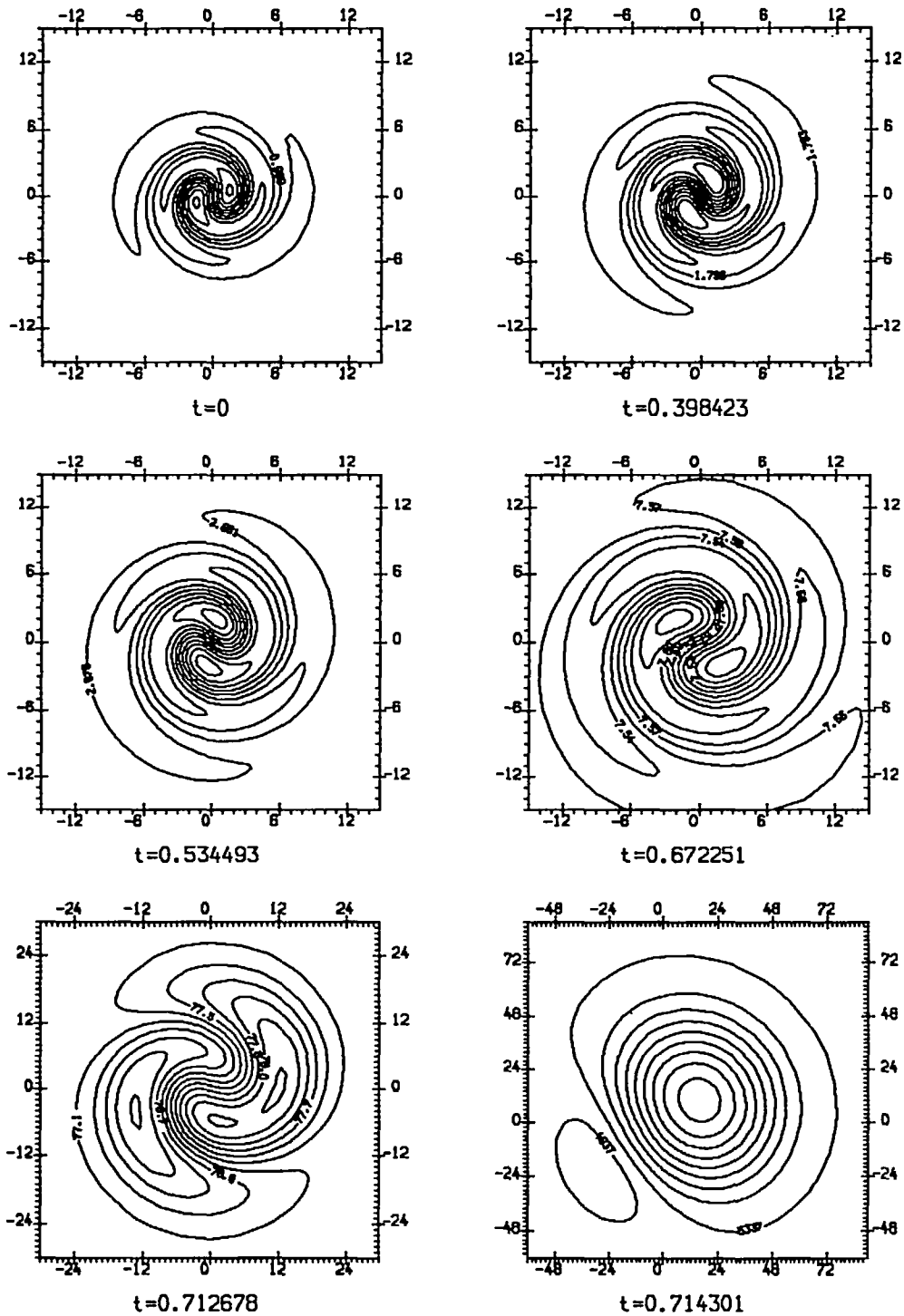


*Figure 2* Evolution in time of the linearized approximation for $\sigma=2$, $\beta=2.4$, $k=1$, $C_o=1$, $\alpha=0.01$

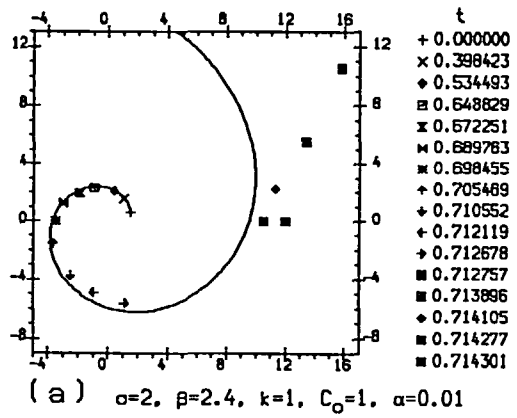


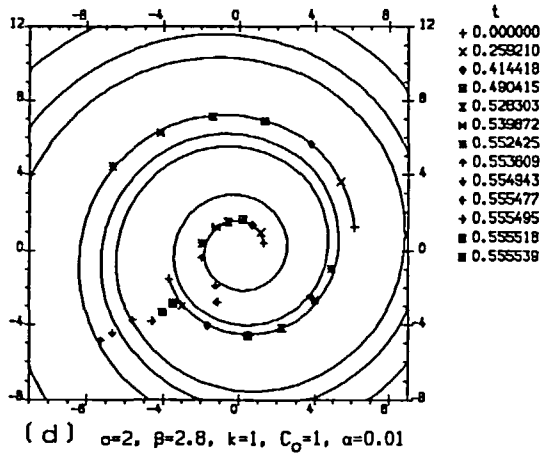


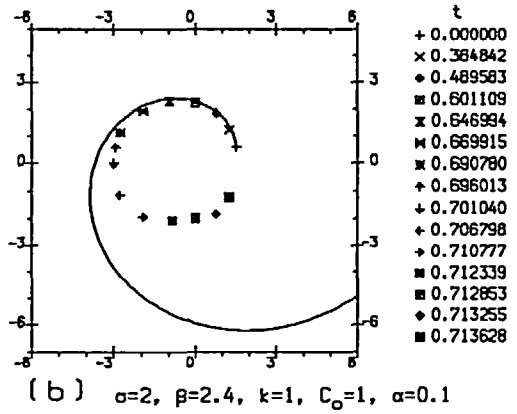


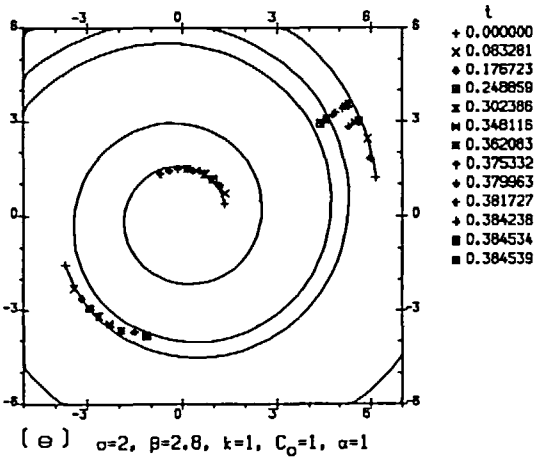


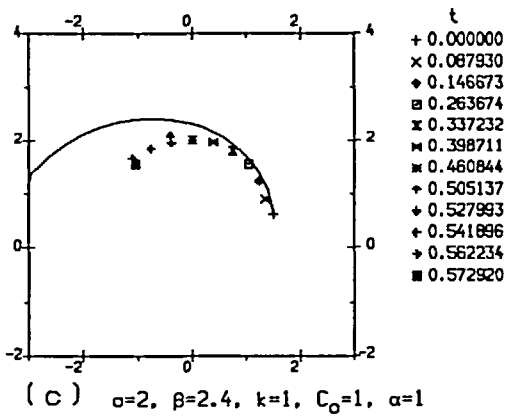


*Figure 3* The self-similar trajectories (the solid lines) and the positions of the local maxima at some times

Here:

$$(u,v)=\iint_{\Omega} ruv\,d\Omega, \qquad A(t;u,v)=\iint_{\Omega} r\frac{\partial g(u)}{\partial r}\cdot\frac{\partial v}{\partial r}+\frac{1}{r}\cdot\frac{\partial g(u)}{\partial \varphi}\cdot\frac{\partial v}{\partial \varphi}\partial\Omega$$

$$g(u)=\int_0^u w^q dw=\frac{u^{\sigma+1}}{\sigma+1}, \qquad f(u)=u^{\beta}$$

$$H=\left\{v:\ r^{1/2}v, \qquad r^{1/2}\frac{\partial v}{\partial r}, \qquad r^{-1/2}\frac{\partial v}{\partial ;}\in L_2. \qquad v(r,0)=v\left(r,\frac{2}{k}\pi\right)\right\}$$

Let $\Omega_h$ be a partition of $\Omega$ into rectangular elements $e_{ij}=[r_i,r_{i+1}]\times[\varphi_j,\varphi_{j+1}]$, $i=1,2,..,l, j=1,2..,m$, $0=r_1<r_2<..<r_{l+1}=R$, $0=\varphi_1<\varphi_2<..<\varphi_{m+1}=\frac{2}{k}\pi$, $S_h$ be the space of continous functions on $\bar{\Omega}$ which are bilinear on each rectangle. Let $\{\psi_{ij}\}_{i=1,j=1}^{l+1\ m+1}$ be the standard basis of $S_h$: $\psi_{ij}(r_i,\varphi_j)=1$, $\psi_{ij}(r_p,\varphi_q)=0$ if $p\neq i$ or $q\neq j$. But, $\psi_{1j}\notin H, j=1,2,..,m+1$ ($r^{-1/2}\psi_{1j,\varphi}\notin L_2$), $\psi_{ij}\notin H$, $i=1,..,l+1$, $j=1,m$, $\left(\psi_{ij}(r,0)\not\equiv\psi_{ij}\left(r,\frac{2}{k}\pi\right)\right)$. That is why we choose:

$$\tilde{\psi}_1=\sum_{j=1}^{m+1}\psi_{1j}=\frac{r_2-r}{r_2}\in H$$

to be a test function instead of $\psi_{1j}$, j=1,2...,m+1. We do this because, if $u$ is interpolated on the basis $\{\psi_{ij}\}_{i=1,j=1}^{l+1\ m+1}$:

$$u_I(t,r,\varphi)=\sum_{i=1}^{l+1}\sum_{j=1}^{m+1}u_{ij}(t)\psi_{ij}(r,\varphi)$$

it is natural that $u_{11}(t)=u_{12}(t)=\ldots=u_{1m+1}(t)$ (we use polar coordinates, so $u(t,0,\varphi)$ must not depend on $\varphi$). Then:

$$u_I=u_{11}\sum_{j=1}^{m+1}\psi_{ij}+\sum_{i=2}^{l+1}\sum_{j=1}^{m+1}u_{ij}\psi_{ij}=u_{11}\tilde{\psi}_1+\sum_{i=2}^{l+1}\sum_{j=1}^{m+1}u_{ij}\psi_{ij}$$

Thus we replace the conditions:

$$(u_t,\psi_{ij})=A)t;u,\psi_{ij}), \qquad j=1,2...,m+1$$

by their sum. In this way the time for solving the problem decreases essentially. To make our trial functions periodic, instead of $\psi_{i1}$ and $\psi_{i(m+1)}$, $i=2,...,l+1$ we choose:

$$\tilde{\psi}_{(i-2)m+2}=\psi_{ij}+\psi_{i(m+1)}$$

The other test functions remain the same:

$$\tilde{\psi}_{(i-2)m+j+1}=\psi_{ij}, \qquad i=2,...,l+1, \qquad j=2,3...,m$$

So our set of trial functions is $\{\tilde{\psi}_i\}_{i=1}^{n}$, $n=lm+1$.

Let $u_h(t,\phi)$ denote the approximate solution:

$$u_h(t,r,\varphi)=\sum_{i=1}^{n}u_i(t)\tilde{\psi}_i(r,\varphi) \tag{27}$$

and let us interpolate the nonlinear functions $g(u)$ and $f(u)$ on the same set of test functions:

$$g_I=I_hg=\sum_{i=1}^{n}g(u_i)\tilde{\psi}_i(r,\varphi), \qquad f_I=I_hf=\sum_{i=1}^{n}f(u_i)\tilde{\psi}_i(r,\varphi) \tag{28}$$

Using (27), (28) and the lumped mass method, our semidiscrete problem may be written in a

matrix form:

$$\tilde{\mathbf{M}}\dot{\mathbf{u}}+\mathbf{K}\mathbf{g}(\mathbf{u})=\tilde{\mathbf{M}}\mathbf{f}(\mathbf{u})$$
$$\mathbf{u}(0)=\mathbf{u}_0$$

or in a normal form:

$$\dot{\mathbf{u}}=-\tilde{\mathbf{M}}^{-1}\mathbf{K}\mathbf{g}(\mathbf{u})+\mathbf{f}(\mathbf{u}) \tag{29}$$
$$\mathbf{u}(0)=\mathbf{u}_0 \tag{30}$$

in which $\mathbf{u}=\mathbf{u}(t)=\{u_1(t), u_2pt(,.., u_n(t)\}^T$, $\mathbf{g}(\mathbf{u})=\{g(u_n)\}^T$, $\mathbf{f}(\mathbf{u})=\{f(u_1),..,f(u_n)\}^T$, $\tilde{\mathbf{M}}$ is the lumped mass matrix:

$$\tilde{\mathbf{M}}=diag\{\tilde{m}_{ii}\}, \qquad \tilde{m}_{ii}=\sum_{j=1}^{n} m_{ij}, \qquad m_{ij}=\iint_{\Omega} r\tilde{\psi}_i\tilde{\psi}_j\,d\Omega$$

$$\mathbf{K}=\{k_{ij}\}, \qquad k_{ij}=\iint_{\Omega} r\frac{\partial\tilde{\psi}_i}{\partial r}\frac{\partial\tilde{\psi}_j}{\partial r}+\frac{1}{r}\frac{\partial\tilde{\psi}_i}{\partial\varphi}\frac{\partial\tilde{\psi}_j}{\partial\varphi}\partial\Omega, \qquad i,j=1,2,...,n$$

Note the two advantages of this method (it is a combination of the so-called 'product-approximation' method[20,21] and the lumped mass method[22]).

- the stiffness matrix $\mathbf{K}$ does not depend on the unknown solution $u(t,r,\varphi)$; so it is calculated only once (only nonzero elements are stored) and is then multiplied by the vector $\mathbf{g}(\mathbf{u})$ at every time step;
- the mass matrix $\tilde{\mathbf{M}}$ is diagonal, so we have not any difficulties in finding $\tilde{\mathbf{M}}^{-1}$ and the system of ODE (29), (30) may be written in normal form.

To solve the system (29), (30), we use a modification of the explicit Runge-Kutta method[23] which is second order accurate in time and has an extended region of stability. The time step $\tau$ is chosen automatically so as to guarantee relative stability and a desired accuracy $\varepsilon$ in the whole time interval.

We have not analyzed theoretically the error of the approximate solution. But we have performed a detailed numerical analysis of the accuracy of the approximate solution. The radially symmetrical case (when $u_\varphi\equiv 0$) is examined in[24], the case of Cartesian coordinates is considered in [25]. In[26] the case of polar coordinates is investigated, but when the solution $u(t,r,\varphi)$ has some axes of symmetry—i.e. the condition $u_\varphi(t,r,0)=u_\varphi\left(t,r,\frac{\pi}{k}\right)=0$ holds instead of (22), (23). The method proposed here is tested on the equation:

$$u_t=\frac{1}{r}(rg_r(u))_r+\frac{1}{r^2}g_{\varphi\varphi}(u)+f(t,r,\varphi), \qquad t>0, \qquad (r,\varphi)\in\Omega \tag{31}$$

with boundary conditions (20)–(23), the initial condition (24) and for $g(u)$ and $f(t,r,\varphi)$, defined below.

*Example 1*

$$g(u)=u, \qquad f(t,r,\varphi)=f_1(r,\varphi)+f_2(r,\varphi)t, \qquad (r,\varphi)\in\Omega, \qquad \Omega=(0,2)\times(0,2\pi),$$
$$f_1(r,\varphi)=1+r(4-r^2)^2 sin(\varphi+r^2)/12,$$

$$f_2(r,\varphi)=\frac{r}{3}[(r^6-8r^4+10r^2+16)sin(\varphi+r^2)-2(3r^4-16r^2+16)cos(\varphi+r^2)], \qquad u_0(r,\varphi)=0$$

In this case the problem (31), (20)–(24) has the exact solution

$$u(t,r,\varphi)=f_1(r,\varphi)t$$

We have calculated the approximate solution $u_h$ using three partitions of $\Omega$ with 64, 256 and

1024 elements respectively. The error:

$$Err_i(t) = \max_{(r,\varphi)\in M_i} |u(t,r,\varphi) - u_h(t,r,\varphi)|, \qquad i = 1,2,3$$

where $M_i$ is the set of the nodes of the i-th partition, decreases four times from one partition to the next:

$$Err_1(t) \approx 4Err_2(t) \approx 16Err_3(t), \qquad \forall t > 0$$

*Example 2*

$f(t,r,\varphi) = f_1(r,\varphi)/(1-t)^2 + f_2(r,\varphi)/(1-t)$, $u_0(r,\varphi) = f_1(r,\varphi)$, $g(u)$, $f_1(r,\varphi)$, $f_2(r,\varphi)$ and $\Omega$ are the same as in the *Example 1*. The test problem has the exact blow-up solution $u(t,r,\varphi) = f_1(r,\varphi)/(1-t)$.

The approximate solution $u_h$ is calculated using the same three partitions of $\Omega$ as in *Example 1*. The experiments show that up to time $t = 0.9900$ the error decreases four times from one partition to the next. The blow-up time $T_0 = 1$ is re-established with accuracy $10^{-15}$.

## CONCLUSIONS

The numerical realization of the blow-up spiral wave solutions of the nonlinear heat-transfer equation with a source shows the possibility for the existence of spiral structures in the corresponding nonlinear medium with parameters $\sigma$ and $\beta$, $\sigma > 0$, $1 < \beta < \sigma + 1$. One very interesting fact we have observed is the self-preservation of these structures (in spite of their closeness to the space homogeneous solution) to more than 99% of their life. Of course the problem for finding the exact eigen functions, describing the spiral propagation of the inhomogeneities in the nonlinear medium, remains an important open one. Moreover,the existence of eigen functions having significant perturbations from the homogeneous solution or even vanishing on infinity is under question. Another interesting problem to be considered is for the case $\beta \geqslant \sigma + 1$.

## ACKNOWLEDGEMENTS

We are very appreciative to Dr V. A. Dorodnitsyn and Dr S. R. Svirshchevskii for having posed the problem and to Prof. S. P. Kurdyumov for the helpful discussions.

This research has been supported by the Ministry of Education and Science, National Foundation for Scientific Research, Bulgaria, under Grant No. MM-6/91.

## REFERENCES

1 Zaikin, A. N. and Zhabotinskii, A. M. Concentration wave propagation in two-dimensional liquid phase self-oscillating system, *Nature* **225**, 535–537 (1970)
2 Alcantara, F. and Monk, M. Signal propagation during aggregation in the slime mold Dictyostelium discoideum, *J. Gen. Microbiolgy*, **85**, 321–334 (1974)
3 Hagan, P. S. Spiral waves in reaction-diffusion equations, *SIAM J. Appl. Math.*, **42**, 762–876 (1982)
4 Koga, S. Rotating spiral waves in reaction-diffusion systems, *Progr. Theor. Phys.*, **67**, 164–188, 454–463 (1982)
5 Greenberg, J. M. Spiral waves for $\lambda$-$\omega$ systems, *SIAM J. Appl. Math.*, **39**, 301–309 (1980)
6 Kuramoto, Y. and Koga, S. Turbulized rotating chemical waves, *Progr. Theor. Phys.*, **66**, 1081–1983 (1981)
7 Kuramoto, Y. and Tsuzuki, T. On the formation of the dissipative structures in reaction-diffusion systems, *Prog. Theor. Phys.*, **54**, 687–699 (1981)
8 Rica, S. and Tirapegui, E. Analytical description of a state dominated by spiral defects in two-dimensional extended systems, *Physica D*, **48**, 396–424 (1991)
9 Galaktionov, V. A., Dorodnitsyn, V. A., Elenin, G. G., Kurdyumov, S. P. and Samarskii, A. A. The quasilinear heat conduction equation with a source: enhancement, localization, symmetry, exact solutions, asymptotic forms and structure, *J. of Soviet Mathematics (JOSMAR)*, **41**, 1163–1356 (1988)

10 Bakirova, M. I., Dimova, S. N. *et al.* Invariant solutions of the heat conduction equation describing directed propagation of combustion and helical waves in a nonlinear medium, *Sov. Phys. Dokl.*, **33**, 187–189 (1988)
11 Akhromeeva, T. S., Kurdyumov, S. P., Malinetskii, G. G. and Samarskii, A. A. *Nonstationary Structures and Diffusion-induced Chaos*, Nauka, Moscow (1992)
12 Samarskii, A. A., Galaktionov, V. A., Kurdyumov, S. P. and Mikhailov, A. P. *Blow-up in Problems for Quasilinear Parabolic Equations*, Nauka, Moscow (1987) (English Trans. Walter de Gruyter, Berlin)
13 Kurdyumov, S. P., Kurkina, E. S., Potapov, A. B. and Samarskii, A. A. Complex multidimensional structures of combustion of a nonlinear medium, *U.S.S.R. Comput. Maths. Math. Phys.*, **26**, 1189–1205 (1986)
14 Koleva, M. G., Dimova, S.N. and Kaschiev, M. S. Anal. of the eigen functions of combustion of a nonlinear medium in polar coordinates by FEM, *Math. Modeling*, **3**, 76–83 (1992)
15 Dimova, S. N., Kaschiev, M. S. and Kurdyumov, S. P. Num. analysis of the eigenfunctions for the combustion of a non-linear medium in the radial-symmetric case, *U.S.S.R. Comput. Maths. Math. Phys.*, **29**, 61–73 (1989)
16 *Handbook of Mathematical Functions*, Ed. M. Abramowitz and I. A. Stegun, Nat. Bur. of Standards, Appl. Math. Series, **55** (1964)
17 Luke, Y. L. *The Special Functions and their Approximations* **1,2**, Academic Press, New-York (1969)
18 Luke, Y. L. On generating Bessel functions by use of the backward recurrence formula, *Aerospace Res. Lab.*, Report ARL72-0030 (1972)
19 Cermak, L. and Zlamal, M. Transformations of dependent variables of the finite element solution of non-linear evolution equations, *Int. J. Num. Meth. Engng.*, **15**, 31–40 (1980)
20 Christie, I., Griffiths, D. F., Mitchel, A. R. and Sanz-Serna, J. M. Product approximation for non-linear problems in the finite element method, *IMA J. Num. Anal.*, **1**, 153–266 (1981)
21 Nie, Y.-Y. and Thomée, V. A lumped mass finite-element method with quadrature for a non-linear parabolic problem, *IMA J. Num. Anal.*, **5**, 371–396 (1985)
22 Novikov, V. A. and Novikov, E. A. Stability control of explicit one step methods for integration of ordinary differential equations, *Dokl. Akad. Nauk SSSR*, **272**, 5, 1058–1062 (1984)
23 Dimova, S. N. and Vasileva, D. P. Lumped mass finite element method with interpolation of the nonlinear coefficients for a quasilinear singular parabolic equation, submitted to *Num. Meth. PDE*
24 Bakirova, M. I., Borshukova, S. N., Dorodnicyn, V. A. and Svirshchevskii, S. R. On the directed heat diffusion in a nonlinear anisotropic medium, Preprint, *Inst. Appl. Math.*, The USSR Acad. Sci., **182** (1985)
25 Vasileva, D. P. Numerical invstigation of the unbounded solutions of a class of quasilinear parabolic equations, *Proc. of XVII Summer School—Varna, Bulgaria, 1991*, 197–200 (1992)